Sound quality analysis of Electric Drive Units under different switching control strategies

M. Glesser[1], S. Ni[1, 2], K. Degrendele[1], S. Wanty[1], J. Le Besnerais[1]

1: EOMYS, 121 rue de Chanzy, F-59260 Hellemmes-Lille, France
2: Univ. Artois, UR 4025, Laboratoire Systèmes Electrotechniques et Environnement, F-62400, Béthune, France

Abstract: Acoustic noise sources in Hybrid Electric Vehicles or full Electric Vehicles (HEV/EV) must be controlled to guarantee an adequate level of acoustic comfort to both passers-by, drivers, and passengers. This article focuses on switching noise resulting from power electronics, also called Pulse Width Modulation (PWM) noise, which may be responsible for unpleasant sounds in Electric Drive Units (EDU). The physics of PWM generation principle is first reminded, from voltage to magnetic excitation harmonics, and noise radiation. An original testbench setup to automatically evaluate the impact of the choice of commutation scheme (e.g., SPWM, SVPWM and DPWM) and frequency is described. Finally, a corpus of motor noise recordings with various PWM strategies is analyzed by means of sound quality metrics and the results are interpreted.

Keywords: sound-quality, electrical machine, e-NVH, PWM, electromagnetic noise

1. Introduction

The interest in electric mobility solutions and particularly Hybrid Electric Vehicles and Electric Vehicles (HEV/EV) has grown significantly in recent years [1], [2], [3]. More and more efforts are made to make those solutions sound pleasant and control their influence on the urban soundscape. This study fits in this objective by questioning the influence of an electric motor control strategy on the sound quality of radiated noise.

The mechanical torque from electric motors is produced by electromagnetic forces arising from magnetic field and magnetic material interactions. However, when the stator is submitted to such forces, and particularly to their harmonics, deflections of the stator-housing assembly may occur, resulting in air-borne noise [4] outside the car, or structure-borne noise in the cabin. Rotor magnetic vibrations may also create structure-borne noise. Large vibration and noise levels can be observed in case of resonance with stator or rotor modes. Two types of magnetic forces can be distinguished in electric motors: slotting forces, depending on the motor topology, and coming from slot to pole interactions, and switching forces, coming from current harmonics induced by power electronics.

Sound power generated by the motor and inverter assembly can be characterized by its overall level in dBA. But the sound quality metrics derived from psychoacoustic studies [5] offer a way to refine sound perception analysis. The influence of e-motor topology on the sound quality has been studied [6], [7], [8]. Some sound quality models combining different psychoacoustic metrics have been built based on jury testing of electric motor noises [9], [10], [11]. Several studies of the sound quality of electric motors compares the impact of using different PWM strategies [7], [12], [13]. However, the comparison is limited to two strategies. The objective of the present study is to extend the comparison to a wider range of PWM strategies used in automotive applications, varying both the switching frequencies and the switching schemes. The physics of PWM noise generation principle is first detailed. A specific experimental setup is then designed and realized to generate a corpus of 288 noise recordings with different PWM strategies. Finally, a sound quality analysis is performed on the sound recordings.

2. PWM noise generation

2.1 PWM voltage and current harmonics

Generally, variable speed traction applications require to generate three-phase variable-frequency Alternative Currents (AC) from the Direct Current (DC) voltage provided by a battery. Pulse Width Modulation (PWM) technique is often used to create a quasi-sinusoidal current at a specified frequency. This technique creates voltage pulses of different duty cycles as shown in Figure 1, based on the comparison of a carrier triangular waveform of frequency fswi (switching frequency) and a modulation waveform of frequency fe (stator current fundamental electrical frequency). Due to the presence of inductances in the electrical circuit, voltage pulses are smoothed and current can increase quasi-sinusoidally as the sliding average of the voltage waveform increases and decreases [14].

This modulation technique creates small magnitude high-frequency harmonics in the voltage and current waveforms. For standard PWM scheme (Sinusoidal PWM, SPMW, or Space Vector PWM, SVPWM), the

frequencies of these harmonics can be described by fPWM = m.fswi ± n.fe where m and n are integers with opposite parity, n > 0 and not multiple of number of phases qs, and fe is the stator current fundamental frequency [16]. An example of this frequency distribution is illustrated in fig 2.1-2. The motor is supplied with PWM control signals (SVPWM switching scheme, fundamental frequency fe = 10 Hz, and switching frequency fswi = 2500 Hz) and the current is measured on one output of the inverter by using an amperometric clamp.

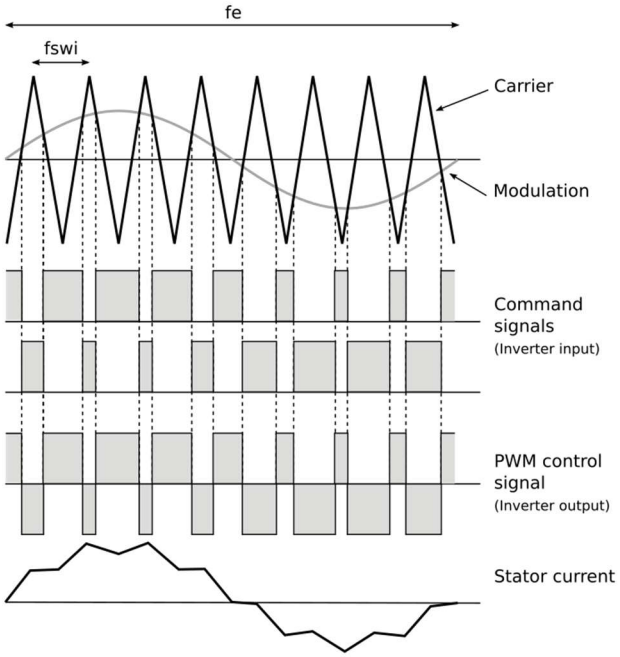

Figure 1: Generation principle of pulse width modulated motor control signal for one phase (bipolar SPWM scheme)

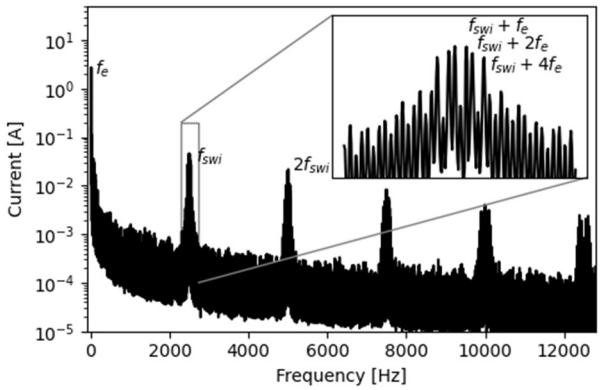

Figure 2: Measured current harmonic for SVPWM switching scheme (fswi = 2500 Hz, fe = 10 Hz)

2.2 PWM force harmonics

Maxwell stress harmonics due to PWM mainly come from the product of the fundamental flux and the PWM flux harmonics of the magnetizing field. The fundamental flux, at the rotor, due to permanent magnets in PMSM (respectively at the stator for induction machines) have a frequency fe and a spatial wavenumber r = p, where p is the number of pole pairs. The spatial wavenumber is referring to a wave distribution along the airgap. It is noted {fe, p}. The largest rotating flux waves due to PWM at the stator can be written as {fPWM, p}. Assuming a symmetrical PWM strategy, the first order of magnetic PWM force waves can be calculated combining these two flux harmonics. Wavenumbers and frequencies of the magnetic force are obtained by adding/subtracting the ones of each flux density wave. For instance, PWM flux wave {-fswi- 2fe, p} = {fswi+ 2fe, -p} and fundamental flux wave {fe, p} produce {fswi+ 3fe, 0} pulsating stress wave and {fswi+ fe, -2p} rotating stress wave.

This harmonic signature can be observed in the noise radiation induced by those forces. The noise radiated by the motor while supplied by the current displayed in fig 2 is plotted in fig 3 as an illustration of such frequency distribution.

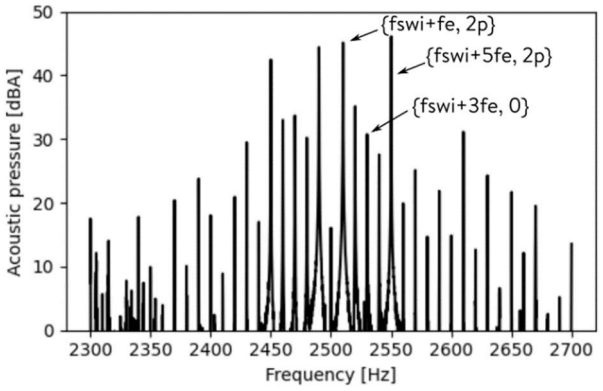

Figure 3: Spectrum of the motor noise with SVPWM switching scheme supply (fswi = 2500 Hz, fe = 10 Hz)

3. Testbench for noise measurement of Electric Drive Units under different switching control strategies

3.1 Testbench description

In order to study the influence of the switching control strategy on the noise produced by an electric motor, a testbench has been set up (see fig 4). A small squirrel cage induction machine (SCIM) machine is controlled with customized programmable PWM strategies. The topology of the machine is: p = 1 pole pairs, Zs = 24 stator teeth and Zr = 28 rotor teeth. The command signals (see fig 2) are generated by a python script. They are sent to a multichannel sound card for digital to analog conversion. After amplification, the command signals are delivered to a 3-phase inverter (2 command signals per phase are needed to control the inverter switches, see fig 1). The inverter generates the PWM control signals from the 44V DC signal provided by the voltage supply. Finally, the motor is supplied with the PWM signals.

The data acquisition system is also controlled by the main python script. It automatically generates control signals with a specific PWM strategy and records the noise produced by the motor in operation. Extensive batch of e-motor sounds with different PWM strategies can be obtained as the testbench is fully automated. Measurements can even be run overnight to reduce background noise level.

The microphone is positioned 20cm away from the motor casing oriented toward a radius passing through the middle of the stator.

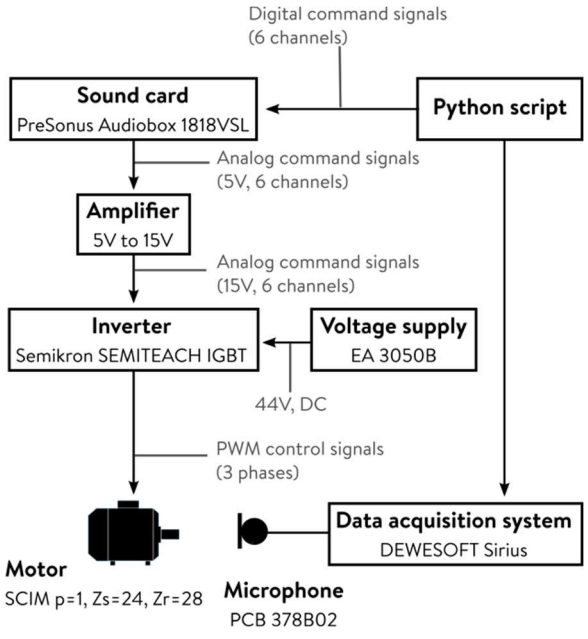

Figure 4: Schematic diagram of the testbench

3.2 Switching strategies

The rotational speed N of the rotor is controlled by the frequency, fe, of the modulation signals (N = 60.fe / p). At a given speed, two parameters of the motor control strategy can be modified: the switching frequency and the switching scheme.

The schemes differ by the modulation waveforms used for the switching [15]. The modulation waveforms of the 8 schemes currently implemented in the testbench are compared in fig 5. As shown in fig 6, the harmonic distribution of the current produced by every switching scheme is different. Consequently, the noise produced by the motor while controlled by every PWM current is different.

In the present study, measurements are performed with a switching frequency of the control signals varying between 2000 Hz and 5500 Hz by steps of 100 Hz. A corpus of 288 recordings (36 switching frequencies x 8 switching schemes) have been acquired and will be analyzed in terms of sound quality in the next sections. All the recordings have been made with a fundamental electric frequency of 10 Hz corresponding to a fixed low speed of the motor (max 60 RPM, depending on the slip).

A modulation index of 0,96 (ratio between the DC voltage to fundamental phase voltage) is chosen to be representative of the cruising mode.

3.3 Sound quality post-processing

The noise recordings have been analyzed by using three sound quality metrics. The loudness according to Zwicker method as standardized in [17] is used to assess the level of the noises in a more subtle way than by using overall dBA level [5]. Loudness indeed considers the non-linear behavior of the auditory system filtering at different noise levels.

The sharpness (from Zwicker loudness and with DIN weighting functions) as standardized in [18] is used to quantify the high frequency content of the recordings, evaluating the feeling of “density” of the sound. The sharpness is inversely related to the sensory pleasantness [5]

Lastly the total prominence ratio (T-PR) is used to quantify the presence of prominent discrete tones in the recordings. The prominence ratio (PR) as standardized in [19] is first determined for each of multiple tonal components in each motor noise spectrum. The total prominence ratio is determined by power summation of the detected prominent tone PR

[20]. The T-PR also tends to be inversely related to the sensory pleasantness.

All sound quality metrics have been computed using MOSQITO open-source python library [21].

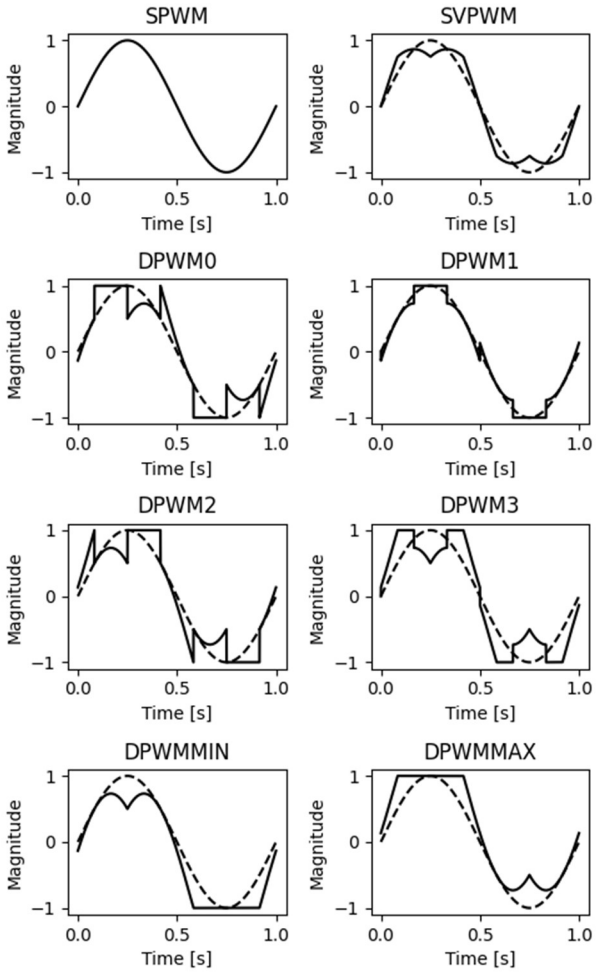

Figure 5: Modulation waveforms of different PWM schemes

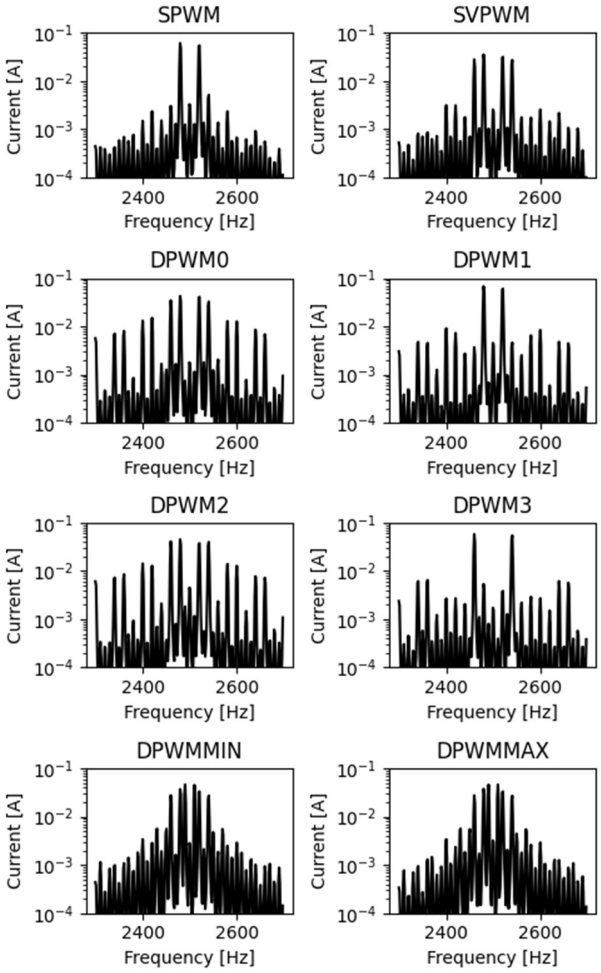

Figure 6: Current harmonic comparison for the different PWM scheme, zoom around fswi (fswi = 2500 Hz, fe = 10 Hz)

4. Results and interpretation

4.1 Switching strategies

The expected slotting harmonics are assessed from the motor topology by using Manatee software [22] quick-Campbell feature (see fig 7). It shows that, when the motor is running at 60 RPM, no significant slotting harmonics are expected for frequencies above 300 Hz.

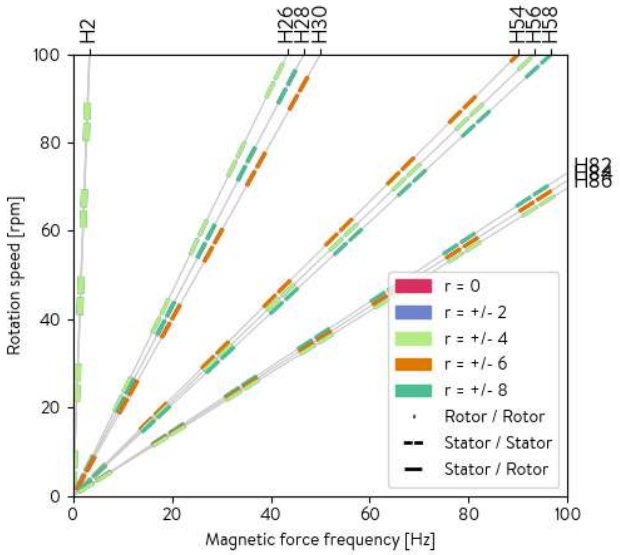

Figure 7: Quick campbell diagram of the slotting forces harmonics expected from a p=1, Zs=24, Zr=28 SCIM machine (with no slip) obtained with Manatee software [22]

Sound spectra measured with different switching frequencies under SPWM are displayed in fig 8.

No significant contribution in the frequency range below 300 Hz is noticed, suggesting that the slotting harmonics are not the main contributor to the noise. The main contribution is rather the group of harmonics around fswi and its multiples due to the switching. Whatever the switching frequency, the noise level around 3600 Hz is systematically higher than the level at other frequencies. This indicates the presence of a structural mode of the motor. It can be noticed that the maximum noise radiation of the motor is reached when the switching frequency matches the natural frequency of the mode.

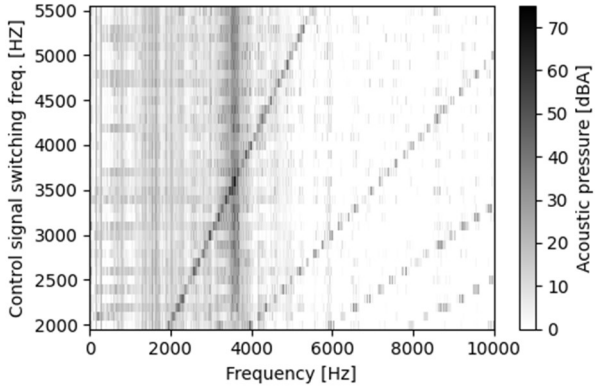

Figure 8: Spectrum of the noise measured with different motor control switching frequencies (fe = 10 Hz, SPWM switching scheme)

4.2 Switching strategy and loudness

The acoustic loudness in sone computed for each of the 288 recordings is displayed in fig 9. For all the switching schemes, the loudness stays below 10 sone as long as the switching frequency is not close to the structural mode (around 3600 Hz). On the contrary, when the switching frequency is close to the mode natural frequency, the loudness is between 20 and 28 sone depending on the scheme. Therefore, the noise radiated by the motor sounds at least twice louder when the switching frequency is close to a natural frequency of the motor structure. However, changing the switching scheme has only a small impact (less than 2 sone) in the level of the radiated noise.

When the switching frequency is close to the natural frequency, it is noticeable that the switching schemes with a highest current peak amplitude (DPWM1, and SPWM) produces louder noise radiation.

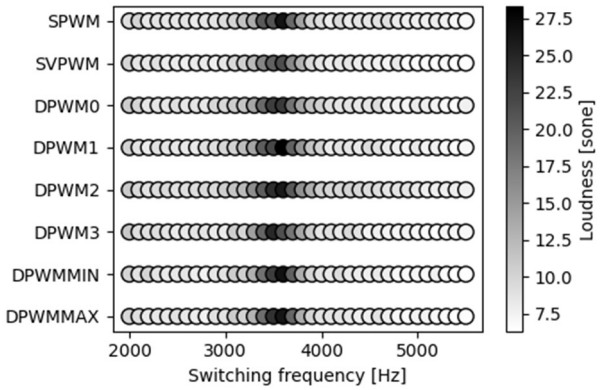

Figure 9: Acoustic loudness of the motor noise under various switching strategy (fe = 10 Hz)

4.3 Switching strategy and sharpness

The acoustic sharpness in acum computed for each of the 288 recordings is displayed in fig 10. The sharpness remains within 1 acum (between 1.8 and 2.8 acum) for all the switching strategies. The sharpest motor noise is only perceived around 1.5 times sharper than the less sharp of the recordings. Sharpness is then not a significant metric to differentiate the recordings of the present study.

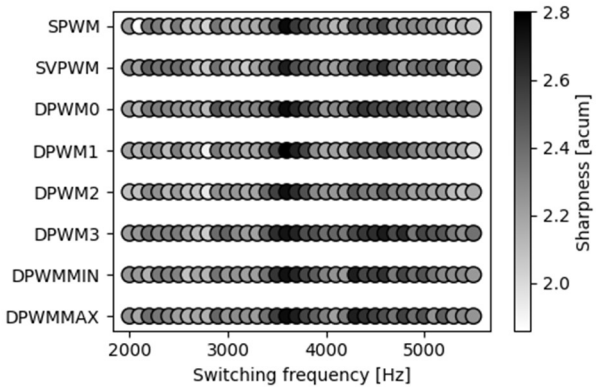

Figure 10: Acoustic sharpness of the motor noise under various switching strategy (fe = 10 Hz)

4.4 Switching strategy and tonality

The total prominence ratio (T-PR) computed for each of the 288 recordings is displayed in fig 11. The T-PR is at least equal to 15 dB. In the frequency range considered in this study, a tonal component is considered as prominent if its PR is above 9 dB. All the recordings can therefore be considered as tonal. Whatever the switching frequency, the PWM schemes with the highest harmonic density around fswi (DPWMMIN and DPWMMAX) are producing the highest T-PR. When the switching frequency is close to the natural frequency, the DPWM0 and DPWM2 schemes produce the lowest T-PR. At a given switching frequency, outside the resonance area, the maximal difference in T-PR between the switching schemes ranges from 5 to 10 dB. If the switching frequency is close to the natural frequency, the difference between the schemes is around 15 dB.

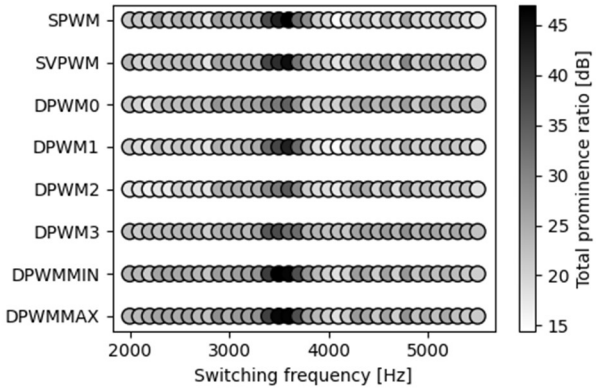

Figure 11: Total prominence ratio (T-PR) of the motor noise under various switching strategy (fe = 10 Hz)

5. Conclusion

The physics of PWM noise generation principle has been presented and illustrated with measured current and noise spectra. Those measurements have been obtained with a dedicated testbench assembled to control a small SCIM machine with diverse PWM control strategies. A corpus of 288 motor noise recordings was generated (8 PWM schemes x 36 switching frequencies) using this setup. The recordings have been analyzed by using the loudness, sharpness and total prominent ratio sound quality metrics.

The acoustic loudness of the radiated noise is more impacted by the proximity of the switching frequency to a structural mode of the machine (loudness can vary by a factor 2) than by a change of the switching scheme (less than 2 sone loudness variation). Sharpness is not a significant metric to differentiate the different motor noises. It stays between 1.8 and 2.8 acum for all recordings. The total prominent ratio is at least equal to 15 dB, making all recordings significantly tonal. The T-PNR is higher if the switching frequency is close to a structural mode of the machine. DPWM2 gives a much lower T-PNR compared to SPWM at resonance.

The testbench is currently being updated to generate a wider range of PWM strategies (including random switching frequency and unipolar switching generation process in particular). Future studies will include the effect of modulation index, as well new sound quality metrics (roughness and tonality hearing model). Finally, the present study will be extended by a jury testing to assess the perceived sound quality of the different recordings.

6. Acknowledgement

The authors acknowledge the contribution of their colleagues to this work.

7. References

[1] Campello-Vicente, H., Peral-Orts, R., Campillo-Davo, N., & Velasco-Sanchez, E.: “The effect of electric vehicles on urban noise maps”, Applied Acoustics, 116, 59–64, 2017.

[2] Eisele, G., Genender, P., & Wolff, K.: “Electric Vehicle Sound design - Just Wishful Thinking?”, Proceedings of Aachen Acoustics Colloquium, 22–24, 2010.

[3] Genuit, K. and Fiebig, A.: “Sound design of electric vehicles - Challenges and risks”, Internoise, Melbourne, Australia, 2014.

[4] Wilamowski, B. M.: “Power electronics and motor drives”, Chapter 9, pp 6-9. CRC Press, 2011.

[5] Zwicker, E., & Fastl, H.: “Psychoacoustics, Facts and Models”, Berlin Heidelberg, Germany, 1992.

[6] Dragonetti, R., Ponticorvo, M., Dolce, P., Di Filippo, S., Mercogliano, F.: “Pairwise comparison psychoacoustic test on the noise emitted by DC electrical motors”, Applied Acoustics, 119, 108–118, 2017.

[7] F. Ramon-Lara, F. Javier Jimenez, Psychoacoustic analysis in the study of the rotating electrical machines noise, in: Proceedings of ICSV22, 2015.

[8] F. Javier Jimenez-Romero, F. Ramon Lara-Raya, M. D. Redel-Macias, Statistical analysis using sound pressure level and sound quality metrics on rotating electrical machines fed by pulse width modulation, 2017.

[9] Fang, Y. and Zhang, T.: “Sound Quality of the Acoustic Noise Radiated by PWM-Fed Electric Powertrain,” IEEE Transactions on Industrial Electronics, vol. 65, no. 6, pp. 4534-4541, June 2018.

[10] Wang, Y., Shen, G., Xing, Y.: “A sound quality model for objective synthesis evaluation of vehicle interior noise based on artificial neural network”, Mechanical Systems and Signal Processing, 45 (1), 255–266, 2014.

[11] Ma, C. et al.: “Sound Quality Evaluation of Noise of Hub Permanent-Magnet Synchronous Motors for Electric Vehicles,” IEEE Transactions on Industrial Electronics, vol. 63, no. 9, pp. 5663-5673, Sept. 2016.

[12] F. Lin, S. Zuo, W. Deng, S. Wu, Noise prediction and sound quality analysis of variable-speed permanent magnet synchronous motor, IEEE Transactions on Energy Conversion.

[13] Andersson, A., Lennström, D. and Nykänen, A.: “Influence of Inverter Modulation Strategy on Electric Drive Efficiency and Perceived Sound Quality,” IEEE Transactions on Transportation Electrification, vol. 2, no. 1, pp. 24-35, March 2016.

[14] Wilamowski, B. M.: “Power electronics and motor drives”, Chapter 11, pp 1-27. CRC Press, 2011.

[15] Yao, F., Geng, L., Janabi, A., and Wang, B., “Impact of modulation schemes on DC-link capacitor of VSI in HEV applications,” 2017 IEEE International Electric Machines and Drives Conference (IEMDC), pp. 1-7, 2017.

[16] Ueda, S.; Honda, K.; Ikimi, T.; Hombu, M.; Ueda, A.: “Magnetic noise reduction technique for an AC motor driven by a PWM inverter”, pp. 470-475, IEEE Trans. Power Electron., vol. 6, no. 3, 1991.

[17] ISO 532-1: “Acoustics — Methods for calculating loudness — Part 1: Zwicker method”, 2017.

[18] DIN 45692: “Messtechnische Simulation der Hörempfindung Schärfe”, 2009.

[19] ECMA-418-1: “Psychoacoustic metrics for ITT equipment — Part 1 (prominent discrete tones)”, december 2020.

[20] ECMA TR/108: “Proposal of new parameters, T-TNR and T-PR for total evaluation of multiple tones”, june 2019.

[21] Martin Glesser. (2021). MOSQITO (v0.3.2). Zenodo. https://doi.org/10.5281/zenodo.5284055

[22] Manatee software, www.manatee-software.com

8. Glossary

AC:	Alternative Current
DC:	Direct Current
EDU:	Electric Drive Unit
EV:	Electrical Vehicle
HEV:	Hybrid Electrical Vehicle
PWM:	Pulse Width Modulation
SPWM:	Sine PWM
SVPWM:	Space Vector PWM
DPWM:	Discontinuous PWM